

# Chromospheric models of dwarf M stars<sup>★</sup>

Pablo J.D. Mauas<sup>1</sup>, Ambretta Falchi<sup>2</sup>, Luca Pasquini<sup>3</sup>, and Roberto Pallavicini<sup>4</sup>

<sup>1</sup> Instituto de Astronomía y Física del Espacio, CC 67, Suc. 28, 1428 Buenos Aires, R. Argentina

<sup>2</sup> Osservatorio Astrofisico di Arcetri, Largo E. Fermi 5, I-50155 Firenze, Italy

<sup>3</sup> European Southern Observatory, La Silla, Casilla 19001, Santiago 19, Chile

<sup>4</sup> Osservatorio Astronomico, Palazzo dei Normanni, I-90134 Palermo, Italy

Received 9 October 1996 / Accepted 18 March 1997

**Abstract.** We present chromospheric models for two dM stars considered as “basal” stars due to the low level of chromospheric activity, and compare them with the model for a very active, flare star obtained in a previous paper. These models are not based on a single spectral feature, but on the continuum in a broad wavelength range (3500 - 9000 Å), on many line profiles corresponding to three different atoms (H, Ca, Na), and on the Mg II h and k flux. We show that a marked chromosphere is present even for stars with the lowest levels of activity, and that the active stars have both a chromospheric temperature rise at larger column mass and a higher chromospheric temperature. These characteristics are responsible for the presence of the Balmer lines in emission in the dMe stars. We also show that the additional energy required to transform a dM star into an active star must be deposited in the high chromosphere, just below the transition region.

**Key words:** stars: atmospheres – stars: chromosphere – stars: late-type

## 1. Introduction

Two thirds of the stars in the Milky Way are M dwarfs. Although their individual masses are small, they account, due to their large number, for half the total mass of main-sequence stars, or about 20% of the luminous mass of the galaxy. Apart from their intrinsic interest, the similarity between solar activity and M dwarf activity suggests that a comparative study can be very valuable for our understanding of phenomena like chromospheric and coronal heating, stellar activity and dynamos.

Generally, dwarf M stars are divided in two subclasses according to whether the Balmer lines are in emission or not. This distinguishes the emission dMe stars from the non-emission dM stars. The presence, in both types, of many atomic lines

and molecular bandheads in absorption, proves the existence of a cool photosphere, whereas the fact that M dwarfs show an emission core in the Ca II resonance lines implies that they have a chromosphere. The difference between the spectra of dM and dMe stars is most likely due to a different chromospheric structure as occurs in quiet and active regions on the Sun.

For a thorough understanding of the atmospheric structure of these stars, complete chromospheric models are needed. Grid of photospheric models for dM stars (from the deep photosphere up to approximately the temperature minimum) were computed by Mould (1976) and more recently by Brett (1995) and Allard and Hauschildt (1995).

The first attempts to model the chromosphere of dM stars where those by Cram & Mullan (1979), who assumed very schematic chromospheric models and studied the response of the emitted Balmer lines to changes of different atmospheric parameters. They found that, as the temperature gradient in the chromosphere increases, the very weak H<sub>α</sub> line predicted for a star with an isothermal chromosphere first becomes an increasingly strong absorption line, then gradually fills in and eventually goes into emission as the chromospheric temperature increases further.

Giampapa et al. (1982) constructed homogeneous models in a similar way, to explain the profiles of the Ca II K line for some representative dMe and dM stars. They found that their models did not predict the right flux for the Mg II resonance lines, and concluded that the assumption of a homogeneous chromosphere was unrealistic.

Houdebine and Doyle (1994a), and Doyle et al. (1994) recently presented grids of atmospheric models, which were merged in Houdebine et al. (1995). They studied the influence of the atmospheric structure on the hydrogen and Ca II line profiles. Houdebine and Doyle (1994b) applied this modelling to the dM2.5e star AU Mic. They obtained very good agreement with the observed profiles for H<sub>α</sub> and H<sub>β</sub>, but they had to add an arbitrary constant to their computed profiles, in order to match them with the observations. In their model, the position of the transition region is fixed to obtain a ratio between the H<sub>α</sub> and the Ly<sub>α</sub> flux of about 1.1, as was found by Doyle et al. (1990).

Send offprint requests to: A. Falchi

\* Tables 4 and 5 are only available in electronic form via <http://cdsweb.u-strasbg.fr/abstract.html>

However, they treated  $\text{Ly}_\alpha$  assuming Complete Redistribution, which has been shown to be a rather poor approximation (e.g. Vernazza et al. 1981).

Hawley & Fisher (1992) computed a theoretical model of the quiescent atmosphere of AD Leo (Gl 388) from the photosphere to the corona. The structure of the corona and the transition region is computed for a loop of length  $L = 10^{10}$  cm and an apex coronal temperature of  $3 \cdot 10^6$  K, in hydrostatic and thermal equilibrium. The photosphere is taken from the grid of models by Mould (1976). The chromosphere is a linear  $\log T - \log m$  interpolation (where  $m$  is the column mass) joining the transition region and the photosphere. They use this model only to determine the quiescent heating rate necessary for the computation of flare models and their results do not fit very well the observed spectral features of the quiet star.

In Paper I of this series (Mauas & Falchi 1994) we presented a semiempirical model for the dM3.5e star AD Leo, computed to match a wide set of observations. We obtained very good agreement for the continuum level, the first four Balmer lines, the Na D and infrared lines and the Mg II flux. However, the agreement was not so good for the Ca II K line profile, and for the  $\text{Ly}_\alpha$  flux, for which we found a difference between the observed and computed features of about a factor of two. The resulting model was used in Paper II (Mauas & Falchi 1996a) as the base for modelling a large flare on the same star.

We believe the approach of semi-empirical modelling, where an atmospheric model is constructed to find the best possible agreement between the computed profiles and a large number of observations, is the one that gives the best results to eliminate the uncertainties found when only a few lines (generally  $\text{H}_\alpha$  or Ca II K) are matched. In a future paper (Mauas & Falchi 1997, Paper IV), we will discuss this problem in detail.

In this paper we present models for two other dM stars, Gl 588 and Gl 628, with photospheric characteristics similar to AD Leo, resulting in very similar colours for the three stars, and we compare the results with the model obtained for AD Leo in Paper I, slightly modified to account for a new set of atomic parameters for the hydrogen model atom.

As Gl 588 and Gl 628 are non-emission stars we expect that the comparison between the chromospheres of the three stars can help understand the mechanisms of chromospheric heating. In particular, we want to understand whether different levels of activity are related to a different chromospheric structure, and/or to different filling factors by a “plage” component, embedded in the same chromosphere (Robinson et al. 1990).

In Sect. 2. we give the stellar parameters of the sample stars, and discuss the observations. In Sect. 3. we explain how the modelling was done, and in Sect. 4. we present the computed models, and compare the predicted and observed spectral features. In Sect. 5. we discuss the energy requirements of the models. Finally, in Sect. 6. we discuss the results.

## 2. The sample stars

The sample consists of two dM stars of the same spectral type: Gl 588 and Gl 628, in addition to AD Leo, already modelled

**Table 1.** Parameters of the sample stars: V magnitude, Cousin B-V, V-R, R-I colours, trigonometric parallax  $\pi$  (in mas), mass M, radius R and gravity g, relative to their solar values, logarithm of the conversion factor C from the observed to surface flux, rotational velocity (in Km/s), and Mg II, Ca II,  $\text{H}_\alpha$  and X-ray surface fluxes in  $\text{erg cm}^{-2} \text{s}^{-1}$ . Negative  $\text{H}_\alpha$  fluxes represent absorption lines.

	AD Leo	Gl 588	Gl 628
Spec. type	dM3.5e (1)	dM3.5 (2)	dM4 (3)
V	9.32 (4)	9.31 (4)	10.08 (4)
B-V	1.53 (4)	1.53 (4)	1.58 (4)
V-R	1.09 (4)	1.06 (4)	1.17 (4)
R-I	1.42 (4)	1.32 (4)	1.52 (4)
$\pi$	204.4(4)	166.5 (4)	242.8 (4)
$R/R_\odot$	0.45 (5)	0.52 (5)	0.33 (5)
$M/M_\odot$	0.4 (4)	0.4 (4)	0.22 (4)
$g/g_\odot$	2.68	1.48	2.02
$\log C$	17.37	17.42	17.5
$v \sin(i)$	5.8 $\text{km s}^{-1}$ (6)		
$F_{\text{MgII}}$	$6 \cdot 10^5$ (1)	$1.1 \cdot 10^5$ (7)	$2.7 \cdot 10^4$ (7)
$F_{\text{CaII}}$	$3.1 \cdot 10^5$ (7)	$2.9 \cdot 10^4$ (8)	$2.2 \cdot 10^4$ (8)
$F_{\text{H}\alpha}$	$1.0 \cdot 10^6$ (1)	$-1.4 \cdot 10^5$ (8)	$-1.2 \cdot 10^5$ (8)
$F_X$	$7.3 \cdot 10^6$ (9)	$3.7 \cdot 10^4$ (9)	$4.1 \cdot 10^4$ (9)

(1) See Paper I

(2) Mathioudakis and Doyle (1992)

(3) Mathioudakis and Doyle (1991)

(4) Legget (1992)

(5) Pettersen (1980)

(6) Marcy & Cheng (1992)

(7) Panagi & Mathioudakis (1993), corrected for the adopted values of  $\log(C)$

(8) Integrated from our flux-calibrated spectra

(9) Fleming et al. (1995)

in Paper I. The main parameters of the three stars are given in Table 1. The data sources are indicated in the notes at the end of the Table. The value  $R/R_\odot$  are calculated using the relation of Pettersen (1980)

$$\log(R/R_\odot) = -0.2092 - 0.2V_J + 0.642(V - R)_J + \log(1/\pi), (1)$$

where the colors in the Johnson system are obtained from those in the Cousin system through the relation given in Legget (1992). The values of  $R/R_\odot$ , that can be obtained with the various relations found in the literature, differ within 10-15% and this uncertainty propagates on the surface flux causing an uncertainty of 20-30%. Gl 588 and Gl 628 are very low activity stars. In particular, Gl 628, with a very low Mg II flux and no detected Ca II flux prior to our observations, had been included in a list of “basal stars” by Mathioudakis et al. (1994). They defined these stars as those that have the minimum level of chromospheric activity. Moreover, Gl 628 is a standard star of the UBV system, but shows long term variability at the 99% confidence level (Weis 1994). Also Gl 588 has been classified as a low activity star by Andrews et al (1990).

AD Leo, on the other hand, is a well known flare star, which shows the Balmer lines in emission, and much larger levels of Mg II and Ca II flux. It has also a much higher X-ray emission

than Gl 628 and Gl 588 (Fleming et al. 1995). We refer the reader to Paper I for a review on the literature on this star.

The spectra we use for Gl 588 and Gl 628 were obtained by us in May and June 1989 at ESO, La Silla. Low resolution spectrophotometry was obtained at the ESO 1.5m telescope equipped with the B&Ch spectrograph in the spectral range 3900-8600 Å. To minimize the effects of slit losses and atmospheric differential refraction, a wide (8 arcsec) slit was used; spectrophotometric standards were observed with the same configuration every night. The data have been reduced using the MIDAS package (Banse et al. 1988) and standard absorption coefficient for La Silla have been adopted. Due to the large slit, the real resolution of the spectra was set by the stellar disk. Although this is slightly variable from one object to another, the intrinsic optical quality of the ESO 1.5m telescope and the hand guiding available at the time of the observations set the stellar image to a diameter of around 2 arcsec, which correspond to a resolution of  $\sim 7$  and  $14$  Å at the blue and red ends of our spectra, respectively. Since the low resolution spectra have been used only to set the basic parameters of the stellar models and to rectify the high resolution echelle spectra, the difference in resolution between the two gratings used in the red and blue part of the spectrum is not relevant for our results.

High resolution spectra were obtained using the CASPEC spectrograph at the 3.6m telescope (Pasquini and D’Odorico 1989). CASPEC was used in combination with the F/1.6 Short Camera. With a slit width of 2 arcsec, the nominal resolving power of this configuration is 18000. The real resolving power has been measured as the FWHM of unsaturated, unblended lines in the comparison (Th-A) spectra, finding values of  $R \sim 24000$ , in good agreement with the nominal one. A spread of 10 % in resolution over each frame is present, due to the intrinsic focus spread of the camera.

In order to minimize the effects induced by possible long term variability in the chromospheric lines, all observations of the same star were performed as close in time as possible, and were completed within one night. The error expected on the absolute calibration of our spectra is about 30 %.

### 3. The modelling

For each star, we computed a different semiempirical model. For “semiempirical” we mean that, given a  $T$  vs.  $z$  distribution, we self-consistently computed non-LTE populations for H, He, Fe, Si, Al, Ca, Na and Mg, solving simultaneously the equations of hydrostatic equilibrium, radiative transfer, and statistical equilibrium.

The modelling was done using the program Pandora developed, and kindly provided to us, by Dr. E. H. Avrett. For a detailed description of the code, we refer the reader to Vernazza et al. (1973, 1981). Avrett et al. (1986) explain in detail how the continuum opacities are treated. We assume that the absorption coefficient for each line has a Voigt profile

$$\phi_\nu = \frac{a}{\pi^{3/2} \Delta\nu_D} \int_{-\infty}^{\infty} \frac{e^{-x^2} dx}{a^2 + (x - (\nu - \nu_0)/\Delta\nu_D)^2} \quad (2)$$

where  $\Delta\nu_D$  is the Doppler width, and  $a$  is the Voigt parameter

$$a = \frac{C_{\text{rad}} + C_{\text{vdW}} \left( \frac{n_{\text{HI}}}{10^{16}} \right) \left( \frac{T}{5000} \right)^{0.3} + C_{\text{Stk}} \left( \frac{n_e}{10^{17}} \right)}{\Delta\lambda_D}. \quad (3)$$

Here  $n_{\text{HI}}$  and  $n_e$  are the atomic hydrogen and electron densities,  $T$  is the electron temperature, and the Doppler width  $\Delta\lambda_D = (\lambda/\nu)\Delta\nu_D$  is in Å units. In the Voigt parameter we include radiative ( $C_{\text{rad}}$ ), and Stark ( $C_{\text{Stk}}$ ) broadening, and Van der Waals ( $C_{\text{vdW}}$ ) broadening due to hydrogen. For the hydrogen lines, we also include natural broadening. For details on how these mechanisms are considered, see Mauas et al. (1988). For hydrogen, the Stark broadening parameters were computed following Sutton (1978), and those for Van der Waals and natural broadening were computed as in Vernazza et al. (1981).  $C_{\text{Stk}}$  for the Na D lines and the Ca II K and H lines are from Konjevic et al (1984), and the  $C_{\text{vdW}}$  are from Lewis et al. (1972), for the Na D lines and from Monteiro et al. (1988), for Ca II K and H. More details on the modelling procedure will be given elsewhere (Mauas & Falchi 1997; Paper IV).

Once the calculations were completed for a given temperature distribution, we computed the continuum intensity and the emerging profiles for different lines, and compared them with the observations. We then modified the assumed  $T$  vs  $z$  distribution, until a satisfactory match between observations and calculations was obtained. The features we used for the comparison were the continuum between 3500 and 9000 Å, the four highest Balmer lines, the Ca II K line, and the Na D lines. Including many different lines removes, or at least reduces greatly, the underdetermination of the models. Moreover, we also checked our predictions against the observed fluxes in the U, B, V, R and I filters and in the infrared.

As can be seen in Table 1, the difference between the gravity values obtained for the three stars is smaller than their uncertainties, and therefore we used  $\log(g) = 4.75$  for our models, as was done for AD Leo in Paper I. This is very similar to the value of  $\log(g) = 4.8$  adopted by the Armagh group for their calculations (e.g. Houdebine and Doyle 1994a).

To our knowledge, there are no estimations for  $v \sin(i)$  for Gl 588 and Gl 628. However, for these inactive stars one should expect values smaller than  $2 \text{ km s}^{-1}$  (Marcy and Cheng 1992). In any case, given the resolution of our spectra, the observed line profiles are dominated by the instrumental broadening, and we did not include in our calculations the effect of rotational broadening.

A very important aspect when modelling cool stars is the inclusion in the opacity calculations of the line blanketing due to the numerous weak lines, both atomic and molecular, of the various species present in the atmosphere, in particular TiO and CaOH (Mould 1976). In this work we included the  $5.8 \times 10^6$  atomic and molecular lines computed by Kurucz (1991).

Houdebine & Panagi (1990) studied the importance of hydrogen atomic parameters on the results of the modelling. In this paper, we used the collisional rates of Johnson (1972), for all transitions except  $\text{Ly}_\alpha$ , for which we used the results by Scholtz et al. (1990), and  $\text{H}_\alpha$  and  $\text{Ly}_\beta$  for which we used the results by

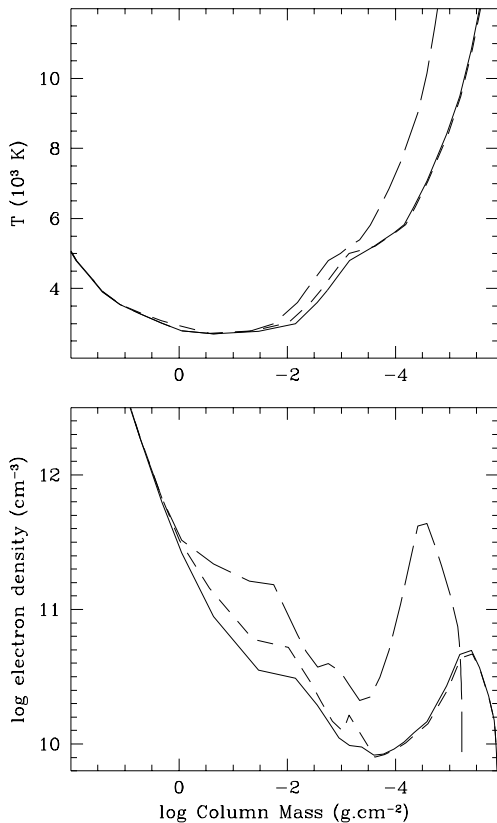


**Fig. 1.** Temperature distribution and electron density for our atmospheric models: full line: Gl 588. Short-dashed line: Gl 628. Long-dashed line: AD Leo (Paper I).

Giovanardi et al. (1987) and Giovanardi & Palla (1989). The Einstein coefficients were also taken from Johnson (1972) and the photoionization cross-sections from Mathisen (1984). The remaining parameters are as in Vernazza et al (1981). We point out that this atomic parameters differ from the ones we used in Papers I and II, were we adopted those in Vernazza et al (1981). For this reason, we have slightly modified the model for AD Leo, to be consistent with the other stars.

#### 4. The results

In Fig. 1 we show the computed models for both stars. For each star, we show the temperature and the electron density as a function of column mass. The atmospheric parameters for the models are given in the Appendix (Tables 4 and 5 are only available in electronic form). For comparison, we also show the model for AD Leo from Paper I, slightly modified due to the use of a new set of atomic parameters for Hydrogen. The new model has a slightly hotter chromosphere, and a chromospheric rise located at a slightly larger column mass than the model in Paper I. In any case, the differences between these two models are much smaller than the differences between AD Leo and the inactive stars.

As can be seen, the photospheric structure of the models for the three stars is very similar, differing only in the upper photosphere, just below the temperature minimum. Given the fact that the three stars have very similar colours (see Table 1), and that the observed continua coincide within the observation and calibration errors, we believe that there is no reason to assume a different structure in the region where the continuum emission is originated (below  $\log(m) \approx 0$ ). The difference just below  $T_{min}$  is due to the fact that the Ca II  $K_1$  minimum is narrower for Gl 628, as will be discussed below.

In Fig. 2 we show our computed continuum, together with the low resolution observations for the three stars between 3500 and 9000 Å. The heads of the most important molecular bands present in our spectra are indicated in Fig. 2. As can be seen, the three stars have a very similar behaviour within the estimated uncertainty of about 30% on our calibrated spectra. Although the general behaviour of the observed spectrum is reproduced within this uncertainty, and many observed spectral features are matched, there are still some molecular bands clearly absent from our calculations, notably CaOH and H<sub>2</sub>O. It can also be noted that the opacity due to TiO seems to be overestimated. Kurucz (1991) cautions against using these opacities to compute the atmospheres of M stars, because they do not include triatomic molecules. However, based on the present results, we believe Kurucz's compilation yields results which are satisfactory enough for our purposes, since we are not interested in fitting any particular feature. In the present calculations, the continuum intensity is needed to account for the photospheric irradiation of the chromosphere, to properly compute the transition rates between levels. We point out that for each line we study in detail, the background opacities around the line were modified in order to match the observed continuum intensity.

In Table 2 we list the observed continuum fluxes for different visible filters (in the Cousin system), together with the values obtained by integrating the computed fluxes with the corresponding filter profile (Schaifers & Voigt 1982). Note the large differences for the visible filters between the fluxes computed with and without Kurucz's opacities, due to the much larger opacity when line blanketing is included. This implies that models based on a fit to filter values computed without taking into account these opacities can be strongly in error. Also shown in Table 2 are the infrared fluxes observed by IRAS, and the corresponding computed values. The computed values lie within the estimated error of the observations.

The profile of the Ca II K line, in particular the  $K_1$  minimum, is a very good indicator of the structure of the temperature minimum (Ayres and Linsky, 1976; Avrett, 1985). In Fig. 3-a we show the profiles of the K line for our models. The computed profiles have been convoluted with the instrumental response (FWHM = 0.18 Å).

In Fig. 3-b we show a detail of the observed profiles. As can be seen, the  $K_1$  minimum is narrower for Gl 628, and thus we had to modify the structure of the upper photosphere, where the inner wings of the line are formed. Also, the fact that the  $K_1$  minimum itself is more intense for Gl 628 implies that the

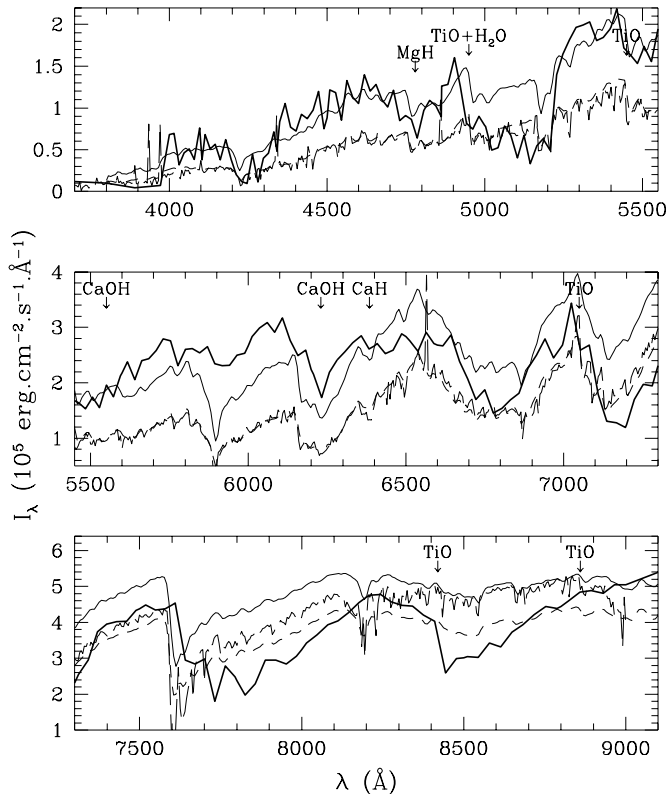


**Fig. 2.** Observed continuum for the three stars (full line: Gl 588. Short-dashed line: Gl 628. Long-dashed line: AD Leo), compared with the computed spectrum (thick line). Note that the three models predict the same continuum emission.

chromospheric rise has to start at a larger column mass for this star than for Gl 588.

In Fig. 4 we show the four lower Balmer lines for both stars: it can be seen that  $H_\gamma$  and  $H_\delta$  have a very low central depth, hidden in the noise. The Balmer lines determine the temperature of the chromosphere. It can be seen in Fig. 4 that the match for these lines is very good, well within the calibration error of the observations. In particular, we were able to reproduce the almost flat profile for  $H_\gamma$  and  $H_\delta$ .

It should be noted that, although in Figs. 3 and 4 we show the relative intensity for clarity, we computed the models to match the absolute intensity at all wavelengths in the line, and we did not need to add any constant to the computed values, contrary to what was done by Houdebine & Doyle (1994b). The relative intensities can match the observations, but both the continuum and line center absolute intensities can differ from the observations.

To check the quality of our models, we also compare the observed profiles of the Na D lines with our computations. The results are shown in Fig. 5. As can be seen, the results are quite good for Gl 588 while for Gl 628 the computed profiles are too narrow, which is a consequence of the larger temperatures in the high photosphere that are needed to reproduce the narrower Ca II line.

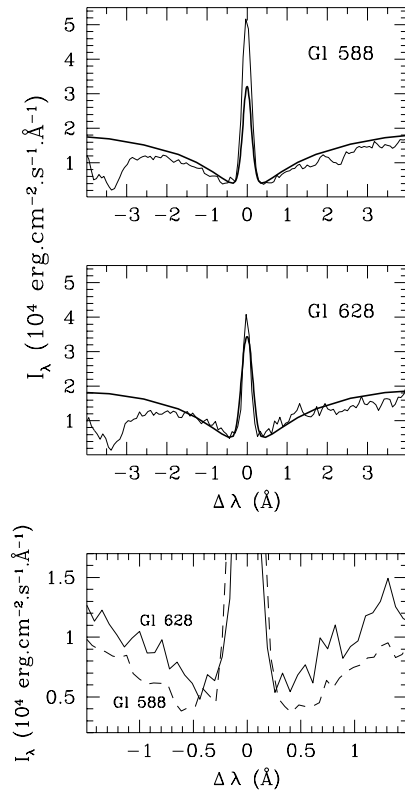


**Fig. 3.** upper panels: Observed (thin line) and computed (thick line) profiles for the Ca II K line. The computed profiles were convolved with the instrumental response. lower panel: Detail of the observed profiles for the Ca II K line. Full line: Gl 628. Dashed line: Gl 588

In Table 3 we list the computed fluxes for the Mg II h and k lines,  $Ly_\alpha$  and  $H_\alpha$  for both stars. For the Mg II resonance lines, the values obtained can be compared with the observations listed in Table 1. Considering the errors in the observed values, and the fact that, without observed line profiles, it is very difficult to study these lines, we believe that the agreement within a factor of 3 is good enough. For  $H_\alpha$ , the agreement with the observed values of Table 1 is very good, as would be expected since the profiles agree very well with the observations. The largest difference is for Gl 628, for which the computed profile is too low. Unfortunately, no observed  $Ly_\alpha$  flux is available for the comparison.

## 5. Energy requirements

One of the main objectives of this kind of atmospheric modelling is to constrain the amount of chromospheric heating required to sustain the atmosphere of the stars, i.e., to balance the radiative losses due to the different spectral lines and continua. Here we compute the radiative cooling rate  $\Phi$  ( $\text{ergs cm}^{-3} \text{s}^{-1}$ ), i.e. the net amount of energy radiated at a given depth by the atmosphere, which is given by

$$\Phi = 4\pi \int \kappa_\nu (S_\nu - J_\nu) d\nu. \quad (4)$$

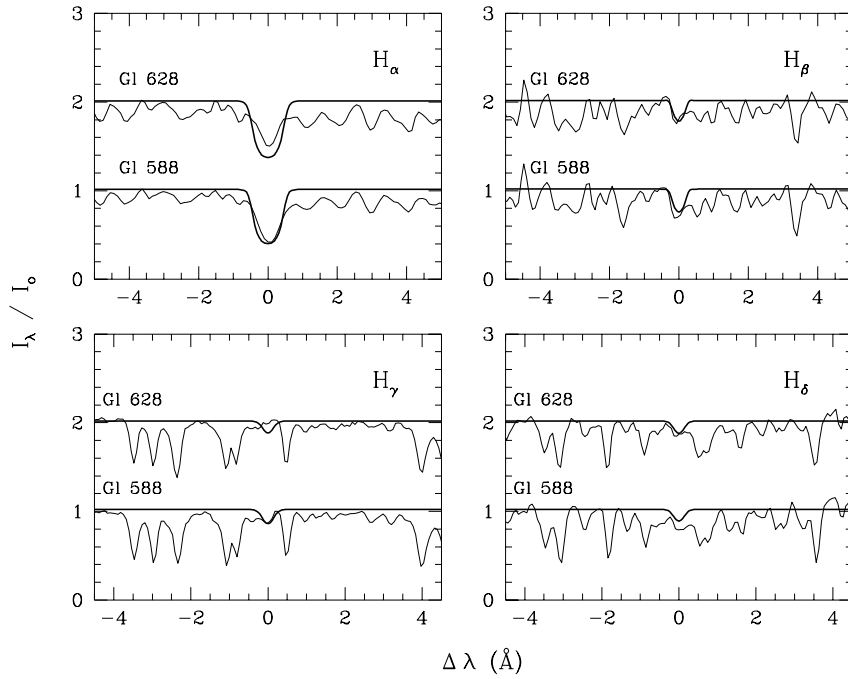


**Fig. 4.** Observed (thin line), and computed (thick line) profiles for the four lower Balmer lines. The relative intensities were displaced for clarity, but the computed continua were the same.

**Table 2.** Observed and computed fluxes at the star surface ( $10^5 \text{ erg cm}^{-2} \text{ s}^{-1} \text{ \AA}^{-1}$ ). For the continuum filters, the first value was computed considering line blanketing, and the second one without it

filter	observed		computed	
	G1 588	G1 628		
B (1)	.80	.45	.65	1.7
V (1)	1.8	1.1	1.7	3.4
R (1)	3.0	1.9	3.0	5.1
I (1)	5.3	4.2	5.1	6.0
12 $\mu\text{m}$ (2)	3.8E-3	3.5E-3	3.4E-3	
25 $\mu\text{m}$ (2)	3.1E-4	2.4E-4	1.9E-4	
60 $\mu\text{m}$ (2)	<3.3E-5	<4.7E-5	5.6E-6	
100 $\mu\text{m}$ (2)	<7.6E-5	<11.1E-5	7.1E-7	

(1) Legget (1992)

(2) Mathioudakis & Doyle (1993)

**Table 3.** Computed line fluxes at the stellar surface ( $\text{erg cm}^{-2} \text{ s}^{-1}$ ). Negative fluxes represent absorption lines.

	G1 588	G1 628
Ly $\alpha$	2.9E5	2.8E5
H $\alpha$	-1.5E5	-1.6E5
Mg II h+k	9.8E4	8.1E4

In this paper we computed the contributions due to  $\text{H}^-$ , H, He I, Mg I and II, Ca I and II, Fe I, Si I, Na I, Al I and CO. The overall results and the most important individual contributions are presented in Fig. 6. A positive value implies a net loss of energy (cooling), and a negative value represents a net energy absorption (heating).

As can be seen, the cooling rate for both stars is very similar, well within the error in the calculations due to differences in the

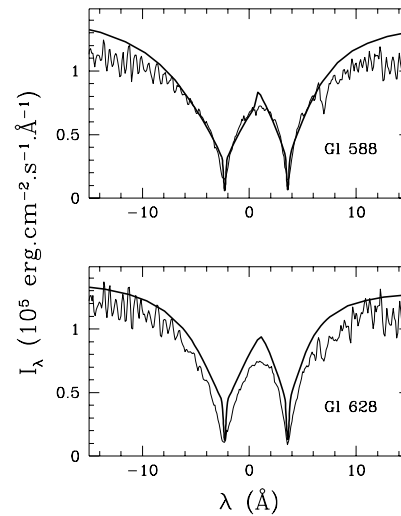


**Fig. 5.** Observed (thin line), and computed (thick line) profiles for the Na D lines.

depth grid. The larger temperature of our model for G1 628 for  $m$  between  $10^{-2}$  and  $10^{-3}$  does not imply a significantly larger radiative loss, since the larger contribution, that of CO, does not vary substantially. In fact, it can be seen in the figure that the cooling rate in the photosphere and the low chromosphere is determined mainly by the balance between  $\text{H}^-$  and CO cooling.

In the temperature minimum region, the  $\text{H}^-$  cooling rate is negative, driving the total rate to negative values. In this case there is a missing *cooling* agent, a fact that was already noted for the Sun, and for AD Leo in Paper I. However, it should be pointed out that almost all cooling is due to CO, which is the only molecule included in the calculations. It seems reasonable

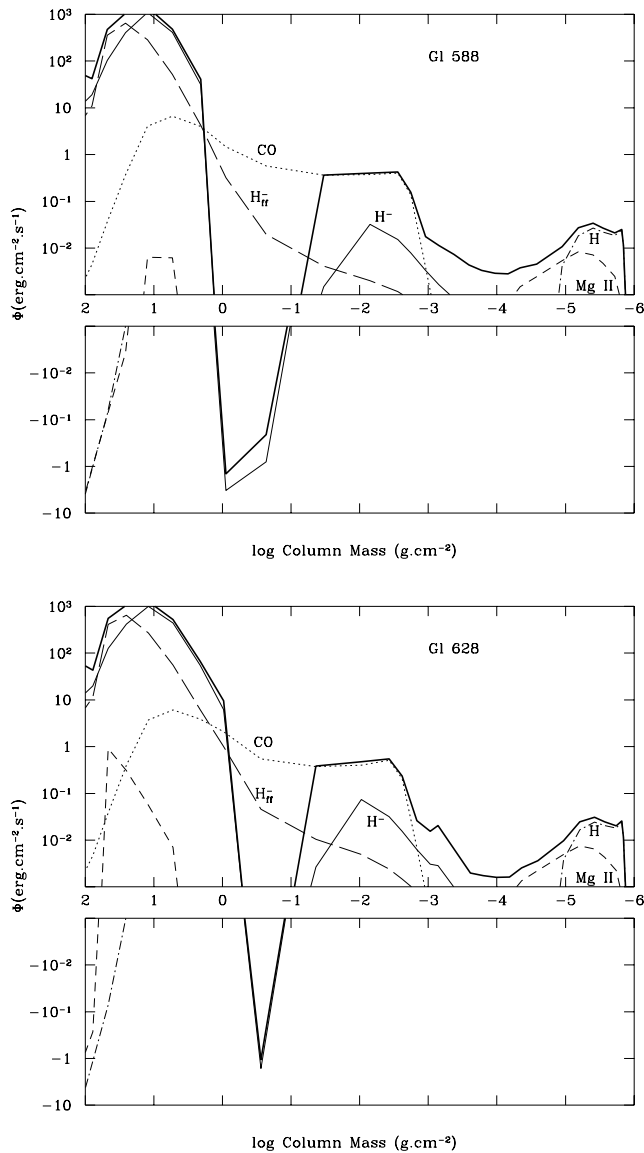


**Fig. 6.** Total radiative cooling rate for our models of Gl 588 (upper panel) and of Gl 628 (lower panel) and the most important contributions to it. Thick line: total rate; dotted line: CO; short-dashed line: Mg II lines; dot-dashed line: H total; long-dashed line:  $H^-$  free-free; thin line:  $H^-$  bound-free.

to expect that, should other molecules be computed in detail, the results would show a similar behaviour as the CO calculations, bringing this region closer to radiative balance.

This results can be compared with the ones shown in Fig. 9 of Paper I, which shows that the dMe star AD Leo has a much larger cooling rate in the high chromosphere, which implies that much more heating is needed to sustain the higher temperature (see Fig. 1). In the mid and high-chromosphere the energy balance is determined by the hydrogen cooling rate and the Mg II rate.

In Fig. 7 we show a detail of the cooling rates in the high chromosphere, that can be compared with Fig. 10 of Paper I. We note that line cooling is positive for all three stars, and it is the most important radiative loss for the cooler stars. In the

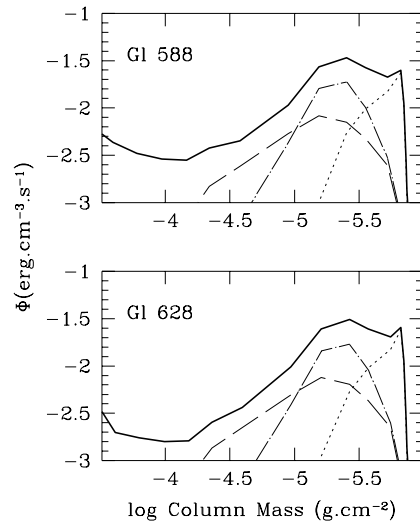


**Fig. 7.** Detail of the chromospheric cooling rates for our models: Gl 588 (upper panel), Gl 628 (lower panel). Thick line: total rate; long-dashed line: Mg II; dot-dashed line: Balmer lines; dotted line: Ly- $\alpha$ .

transition region, for temperatures larger than 15000 K, Ly $\alpha$  is the most important cooling agent, whereas at lower temperatures the Balmer lines become dominant. In this region, cooling in the  $H_\alpha$  line is three times larger than in  $H_\beta$ , and ten times larger than for  $H_\gamma$  to  $H_8$  together. As the temperature drops further, Mg II h and k lines become important. Ca II H and K cooling, on the other hand, is an order of magnitude smaller than Mg II cooling.

## 6. Discussion

In this paper we presented chromospheric models for two M dwarf stars considered as “basal” stars due to the very low level of chromospheric activity, to be compared with the model for a very active, flare star, computed in Paper I. These models are not based on a single spectral feature, but on many lines corresponding to three different atoms, the continuum in a broad wavelength range, from the ultraviolet to the infrared, and the Mg II h and k flux. All in all, the agreement between models and observations is remarkably good.

As can be seen in Fig. 1, the main difference between the two dM stars can be found in the structure of the initial chromospheric rise, just above the temperature minimum. This explains the higher intensity of the  $K_1$  minimum for Gl 628. However, this difference is not reflected in a larger cooling rate at these heights, and is not important from an energetic point of view.

There is a slight difference (about 100 K at  $\log(m) = 0$ ) between the high photosphere of Gl 628 and the others, to fit the narrower  $K_1$  of Gl 628. On the other hand, this modification made the fit to the Na D lines worse for Gl 628 than for Gl 588. In general, the overall fit for Gl 628 is not as good as for Gl 588, suggesting that there might be some problems with the modelling of this star. However the difference in the high photosphere of Gl 628 does not affect the continuum emission

that originates in lower layers, and we can conclude that the observations are compatible with the assumption of a similar photosphere for the three stars.

Considering that both GI 588 and GI 628 were classified as “basal” stars, it should be noted that even in these cases there is a marked chromosphere, well above a radiative equilibrium atmosphere. This confirms the conclusions of other authors (e.g. Cram & Mullan 1979; Giampapa & Liebert 1986).

Comparing the dM and the dMe stars, we can see that, as expected, the presence of the Balmer lines in emission (and the much larger Ca II and Mg II fluxes) is determined by the structure of the chromosphere, much hotter for AD Leo than for the other two stars. This, in turn, implies a much larger electron density, and a closer coupling of the source function with the Planck function. In fact, the model for AD Leo is 2000 K hotter than the ones for the dM stars, at  $\log(m) = -4$ .

From an energetic point of view, it can be seen comparing the results presented here with the ones in Paper I, that the additional energy required to transform a dM star into an active star is needed in the high chromosphere, just below the transition region. The mid-chromosphere, in turn, is automatically heated by the energy emitted above it, and reabsorbed in this region, in particular, in the Mg II and Balmer lines.

*Acknowledgements.* We would like to thank the referee, Dr. S. Hawley, for constructive criticisms that helped to improve the paper.

## Appendix A

The atmospheric parameters for our models are given in Tables 4 and 5. The columns give the column mass in  $\text{g cm}^{-2}$ , the electron temperature in K, the microturbulent velocity in  $\text{km s}^{-1}$ ; the continuum optical depth at  $5000 \text{ \AA}$ ; the hydrogen, proton, and electron density in particles per  $\text{cm}^{-3}$ ; and the height  $h$  (in km) above the level where  $\tau_{5000\text{\AA}} = 1$ . The atmospheric parameters for these models are available upon request, through electronic mail.

## References

- Allard F., Hauschildt P.H., 1995, ApJ, 445, 433  
 Allen C.W., 1963, “Astrophysical Quantities”, Athlone.  
 Andrews, A.D., Zembrowski, P.J., Houdebine E.R., 1990, A&A, 235, 264  
 Avrett E.H. 1985, in *Chromospheric diagnostic and modelling* ed. B. Lites, p.67  
 Avrett E.H. , Machado, M.E., Kurucz R.L. 1986, in *The Lower Atmosphere in Solar Flares*, ed. D.F. Neidig, p. 216  
 Ayres, T.R., Linsky, J.L., 1976, ApJ, 205, 874  
 Banse, K., Grosbol, P., Ponz, D. et al., 1988, The MIDAS Image Processing System, in: *Instrumentation for Ground Base Astronomy: Present and Future*, ed. L.B. Robinson, (Springer)  
 Brett J.M., 1995, A&A, 295, 736  
 Cram L.E., Mullan D.J., 1979, ApJ, 234, 579  
 Doyle J.G., Butler, C.J., 1990, A&A, 235, 335  
 Doyle J.G., Houdebine E.R., Mathioudakis M., Panagi P.M., 1994, A&A, 285, 233  
 Doyle J.G., Panagi P.M., Byrne, P.B. 1990, A&A, 228, 443  
 Fleming T.A., Schmitt J.H.M.M., Giampapa M.S., 1995, ApJ, 450, 401  
 Giampapa M.S., Liebert, J., 1986, ApJ, 305, 784  
 Giampapa M.S., Worden S.P., Linsky, J.L., 1982, ApJ, 258, 740  
 Giovanardi, C., Natta A., Palla F., 1987, A&AS, 70,269  
 Giovanardi C., Palla F., 1989, A&AS, 79, 157  
 Hawley S.L., Fisher G.H., 1992, ApJS 78, 565  
 Houdebine E.R., Doyle J.G. 1994a, A&A, 289, 169  
 Houdebine E.R., Doyle J.G. 1994b, A&A, 289, 185  
 Houdebine E.R., Doyle J.G., Kościelicki M., 1995, A&A, 294, 773  
 Houdebine E.R., Panagi P.M., 1990, A&A, 231, 459  
 Johnson, L.C., 1972, ApJ, 174, 227  
 Konjevic N., Dimitrijevic M., Swiese W.L., 1984, J.Phys.Chem. Ref.Data 13, 649  
 Kurucz R.L. , 1991, in: *Precision Photometry: Astrophysics of the Galaxy*, eds. A.G. Davis Philip, A.R. Upgren, and K.A. Janes, L. Davis Press, Schenectady  
 Legget S.K., 1992, ApJS 82, 351  
 Lewis, E.L. McNamara L.F., Michels, H.H., 1972, Sol.Phys. 23, 287  
 Mathioudakis M., Drake J.J., Vedder P.W., Schmitt J.M., Bowyer S., 1994, A&A, 291, 517  
 Mathioudakis M., Doyle J.G. 1991, A&A, 244, 433  
 Mathioudakis M., Doyle J.G. 1992, A&A, 262, 523  
 Mathioudakis M., Doyle J.G. 1993, A&A, 280, 181  
 Mathisen, R., 1984, Institute of Theoretical Astrophysics, Publication Series No. 1  
 Marcy, G.W., Cheng, G.H., 1992, ApJ, 390, 550  
 Mauas P.J. , Avrett E.H. , Loeser R. 1988, ApJ 330, 1008  
 Mauas P.J. , Falchi, A. 1994, A&A, 281, 129 (Paper I)  
 Mauas P.J. , Falchi, A. 1996a, A&A, 310, 245 (Paper II)  
 Mauas P.J. , Falchi, A. 1997, A&A, in preparation (Paper IV)  
 Monteiro T.S., Danby E.L., Cooper I.L., Dickinson A.S., Lewis E.L., 1988, J.Phys.B 21, 4165  
 Mould J.R., 1976, A&A, 48, 443  
 Pasquini, L., D’ Odorico, S., 1989, The ESO Cassegrain Echelle Spectrograph, ESO Operating Manual N. 2  
 Pettersen B.R., 1980, A&A, 82, 53  
 Robinson, R.D., Cram L.E., Giampapa M.S., 1990, ApJS 78, 891  
 Schaifers, K., & Voigt, H.H., 1982, Numerical Data and Functional Relationships in Science and Technology, vol. 2, p. 52-79.  
 Scholz, T.T., Walters, H.R.J., Burke, P.J., Scott, M.P., 1990, MNRAS, 242, 692  
 Sutton K., 1978, J.Q.S.R.T. 20, 333  
 Vernazza, J.E., Avrett E.H. , Loeser R. 1973, ApJ 184, 605  
 Vernazza, J.E., Avrett E.H. , Loeser R. 1981, ApJS 45, 635  
 Veeder, G.J., 1974, AJ, 79, 1056  
 Weis, E.W., 1994, AJ, 107, 1135